ACS APPLIED MATERIALS & INTERFACES

Research Article

www.acsami.org

Structural and Equilibrium Effects of the Surface Passivant on the Stability of Au Nanorods

Nicholas A. Merrill,[†,∥] Manish Sethi,[‡,§,∥] and Marc R. Knecht*[,†]

[†]Department of Chemistry, University of Miami, 1301 Memorial Drive, Coral Gables, Florida 33146, United States

[‡]Department of Chemistry, University of Kentucky, 101 Chemistry-Physics Building, Lexington, Kentucky 40506-0055, United States

Supporting Information

ABSTRACT: Au nanomaterials are well-known for their optical properties, where Au nanorods have demonstrated unique capabilities because of their readily tunable size and shape. Unfortunately, functionalization of the material surface is challenging because of their lack of stability after only a few purification cycles. Here, we demonstrate that enhanced Au-nanorod stability can be achieved by purifying the materials using dilute cetyltrimethylammonium bromide (CTAB) wash solutions. To this end, purifying the materials in such a manner shifts the passivant on/off equilibrium to maintain surfactant adsorption to the metal surface, leading to enhanced stability. Interestingly, from this study, a bimodal distribution of Au nanorods was evident, where one species was prone to bulk aggregation, whereas the second population remained stable in solution. This likely arose from defects within the CTAB bilayer at the nanorod surface, resulting in selective material aggregation. For this, those structures with high numbers of defects aggregated, whereas nanorods with a more pristine bilayer remained stable. Coating of the Au nanorods using polyelectrolytes was also explored for enhanced stability, where the composition of the anionic polymer played an important role in controlling materials stability. Taken together, these results demonstrate that the stability of Au nanorods can be directly tuned by the solvent-exposed surface structure, which could be manipulated to allow for the extensive material functionalization that is required for the generation of nanoplatforms with multiple applications.

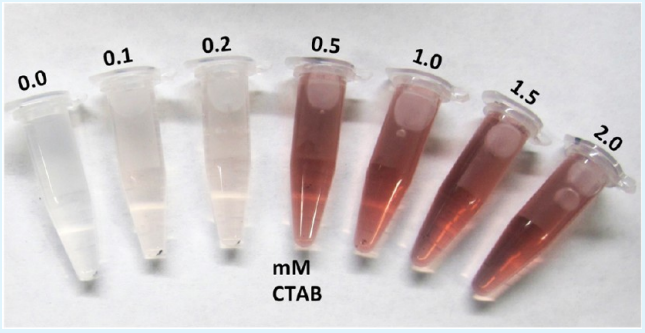

KEYWORDS: *Au nanorods, CTAB, stability, polymers, chemical functionalization*

INTRODUCTION

Au nanorods represent targets for a variety of applications ranging from bioanalytical detection to building blocks for electronic-device components.[1−6] The interest in these materials arises from their unique properties that are directly controlled by the material shape and structure.[7−11] To that end, the inorganic core and the surface passivant, typically composed of the surfactant cetyltrimethylammonium bromide (CTAB), act in concert to control the optical, electronic, conductive, and recognition properties while maintaining material stability.[9,11−14] Au nanorods possess two distinct plasmon bands associated with the asymmetric structure of the materials: one corresponding to the transverse axis, known as the transverse surface plasmon, and one corresponding to the longitudinal axis, termed the longitudinal surface plasmon.[8,9,11] The longitudinal surface plasmon is highly sensitive to the aspect ratio of the Au nanorods such that increasing this ratio results in a red shift of the absorbance.[12] Although multiple mechanistic aspects have been proposed for the synthesis of Au nanorods using CTAB, it is clear that a surfactant bilayer is generated at the surface of the materials, imparting a significant positive charge.[11,15−17] As a result of this cationic layer, the materials remain stable in aqueous solution because of electrostatic repulsion effects between the individual nanorods.[18]

Although extensive studies have focused on exploiting the inherent properties of the metallic core, the CTAB passivant is also integral to the activity of the Au nanorods.[6,8,19−21] To this end, it is exposed to solution and thus interacts with other reagents and species in the mixture, and it can be modified to incorporate additional chemical functionalities for selected applications.[3,8,22−24] Furthermore, the surfactant molecules in the bilayer routinely exchange from the nanorod surface with additional ligand molecules in solution, which has been recently exploited to incorporate secondary ligands.[18,25] Unfortunately, the CTAB layer has three main drawbacks: it can be difficult to fully exchange with secondary ligands, the surfactant molecules are known to be toxic to cells when released from the nanorod surface, and the exact structure of the surfactant bilayer at the nanorod surface remains unclear.[11,26−28] Although it is possible to preferentially conjugate new ligands at the tips of Au nanorods,[2,29] displacement of the surfactant monolayer along

Received: May 24, 2013
Accepted: July 19, 2013
Published: August 6, 2013

the longitudinal axis remains challenging. A few methods have demonstrated the ability to displace CTAB with secondary thiol-based ligands along this region of the metallic surface;[30−32] however, Raman studies of the materials after the exchange process suggest that a portion of the toxic CTAB layer remains.[33] Furthermore, nanorod stability during these exchange processes remains a significant concern. To this end, multiple washing steps are required before and after secondary-ligand conjugation to remove unbound molecules. This can cause a shift in the ligand on/off equilibrium, resulting in the release of the passivant from the Au nanorod and eventual material destabilization.[18] This is especially important for the CTAB-coated rods that are known to aggregate after only two to three centrifuge-based washing steps, which are required to ensure removal of the excess toxic surfactant.[18] To enhance the functionalization and eventual application of Au nanorods, it is critically important to fully characterize the ligand layer and develop chemical functionalization procedures that maximize material stability. This would ideally allow for multistep ligand-coupling procedures that would otherwise be prohibited resulting from nanorod instability. This is especially true for biological applications where multiple material surface functionalization steps with polymers,[3] proteins,[34] antibodies,[19,35] and other biomacromolecules[36] are typically required.

Here, we present evidence to suggest that defects within the CTAB bilayer on Au nanorods play an important factor in mediating the stability and functionalization capabilities of the materials. In this regard, individual nanorods with a higher number of imperfections in the bilayer destabilize and aggregate first, whereas those materials with well-defined bilayer structures remain stable in solution and thus give rise to a bimodal material population. This effect was probed on the basis of the concentration of free surfactant in solution, which was controlled by the number of individual washing steps performed on the system and the surfactant concentration of the wash solution. For this, the materials were washed with increasingly concentrated CTAB wash solutions to elucidate a concentration at which the materials remained stable after multiple purification cycles. After each wash, the materials were analyzed by UV−vis, transmission electron microscopy (TEM), dynamic light scattering (DLS), and ζ-potential analysis. The results demonstrate that for samples where aggregation and material precipitation were present a significant population of the original Au nanorods remained. Furthermore, when the materials were washed with a dilute CTAB solution of $\geq$0.5 mM, the majority of the materials remained stable after at least 10 wash cycles, suggesting that they could be extensively chemically functionalized without leading to destabilization. Polyelectrolyte (PE) coating of the nanorods was then probed to ascertain the enhanced stability of the coated materials, and purification analysis demonstrated that the polymers could be removed from the Au surface, leading to materials precipitation. An additional correlation was noted that indicated that the PE structure affected the stability of the materials in which the changing of the functionality resulted in altered nanorod stability. To this end, polystryrene sulfonate (PSS)-coated Au nanorods remained stable after significantly more purification cycles compared to their counterparts coated with poly(acrylic acid) (PAA), allowing for additional functionalization steps that would require multiple purification cycles. Together, these results present important implications for the ability to functionalize Au nanorods as well as demonstrate new methods for their long-term stability, of which both are important to generate future multifunctional nanoplatforms.

EXPERIMENTAL SECTION

Chemicals. $HAuCl_4 \cdot 3H_2O$, CTAB, NaCl, poly(acrylic acid), and polystyrene sulfonate were purchased from Sigma-Aldrich. $NaBH_4$ was purchased from EMD, ascorbic acid was acquired from J. T. Baker, and $AgNO_3$ was purchased from BDH. All chemicals were used as received without additional purification. For all experimentation, Milli-Q water (18 MΩ cm; Millipore) was used.

Preparation of the Au Nanorods. For the fabrication of the Au nanorods, the two-step, seed-mediated method was employed.[2,18,37] In the first step, Au nanoparticle seeds were prepared as follows: 250 μL of a 10.0 mM aqueous $HAuCl_4$ solution was added to a plastic conical centrifuge tube. To this, 7.50 mL of a 100 mM aqueous CTAB solution was added. The mixture of these reagents changed the solution color from bright yellow to deep orange. To this, 600 μL of a freshly prepared, ice-cold 10.0 mM $NaBH_4$ solution was added, which immediately changed the solution color to pale brown. The reaction was then left undisturbed for ∼3.0 h to ensure complete Au^{3+} reduction; however, the seeds were discarded 5.0 h after synthesis.

After seed generation, Au nanorods were prepared on a 50.0 mL scale. For this, 47.5 mL of 100 mM CTAB was mixed with 2.0 mL of 10.0 mM $HAuCl_4$ in a conical centrifuge tube. To this, 300 μL of 10.0 mM $AgNO_3$ and 320 μL of 100 mM ascorbic acid were added. All of these solutions were freshly prepared, added to the reaction in the listed order, and the system was mixed by inversion after the addition of each solution. Finally, 210 μL of the Au seed solution was added followed by gentle mixing, after which the reaction was left undisturbed for at least 3.0 h at 25.0 °C before use.

Nanorod Purification Stability Analysis. CTAB solutions of different concentrations were prepared by the aqueous dilution of a 40.0 mM CTAB stock in water to result in final concentrations of 0.1, 0.2, 0.5, 1.0, 1.5, and 2.0 mM. Samples (1.00 mL) of the crude Au nanorods were then centrifuged at 14 000 rpm for 9.0 min in microcentrifuge tubes. The clear and colorless supernatant was discarded, and each pellet containing the Au nanorods was redispersed using a selected concentration of CTAB wash solution. The nanorods were subsequently centrifuged nine times, and the pellets were redispersed in the same CTAB solution. All Au nanorods were analyzed between each washing step using the techniques described below.

Nanorod Polyelectrolyte Surface Coating. PE coating of the Au nanorods was studied using poly(acrylic acid) of 8 000 g/mol (PAA8, 45 wt %) and 15 000 g/mol (PAA15, 35 wt %) as well as polystyrene sulfonate of 75 000 g/mol (PSS, 18 wt %). Stock solutions of 10 mg/mL of PE were prepared using a 10.0 mM NaCl solution, which were discarded after 1 week. Coating of the materials followed previous layer-by-layer methods.[3,38] Briefly, 1.0 mL Au-nanorod samples were centrifuged at 14 000 rpm for 9.0 min. The supernatant was discarded, and the pellet was redispersed in 1.00 mL of 0.5 mM CTAB and centrifuged again. After the supernatant was discarded for the second time, the pellet was redispersed in 700 μL of H_2O. To each sample, 200 μL of the 10 mg/mL PE solution was added along with an additional 100 μL volume of 10.0 mM NaCl, raising the final volume to 1.00 mL. The coating solutions were mixed thoroughly using a vortexer for ∼3 s and were then incubated on a thermomixer at 700 rpm for 2.0 h at room temperature. After complete PE coating, the samples were centrifuged at 11 000 rpm for 10.0 min, the supernatant was removed, and the pellet was redispersed in 1.0 mL of water. The samples were successively centrifuged and redispersed in water four times and analyzed after each wash.

Characterization. UV−vis spectra were obtained using an Agilent 8453 UV−vis spectrometer, employing 2.00 mm path-length quartz cuvettes (Starna). Prior to use, the cuvettes were fully cleaned using aqua regia and rinsed thoroughly with water to remove any trace acid. Note that aqua regia is extremely caustic and extra precaution should be taken. All spectra were background subtracted against water, which was the only solvent used. TEM images were obtained using a JEOL

2010F transmission electron microscope operating at 200 kV. To prepare the TEM sample, 5.00 μL of the Au-nanorod solution was pipetted onto the thin carbon surface coated onto a 400 mesh Cu grid (EM Sciences). The sample was allowed to dry overnight prior to imaging. Solution-based ζ-potential and DLS analyses were completed using a Zetasizer Nano ZS System (Malvern, Inc.).

RESULTS AND DISCUSSION

Au nanorods were synthesized using the seed-mediated method where high concentrations of CTAB are required (~100 mM).[37] Under the selected conditions, materials with an overall size of 27 ± 11 nm by 79 ± 24 nm are typically prepared, with an aspect ratio of 2.93. To study the stability of the Au nanorods for multistep surface functionalization, the materials were purified using wash solutions of selected dilute surfactant concentrations of ≤2.0 mM. Such solutions were anticipated to control the on/off equilibrium of the CTAB on the nanorod surface. Under this assumption, the equilibrium should be shifted at a critical surfactant concentration so that the passivant remains adsorbed, leading to the stabilization of the materials after multiple washing cycles.

To study the on/off equilibrium effect of the CTAB passivant, the Au nanorods were washed multiple times. In this sense, the materials were centrifuged to form a pellet, the supernatant was decanted, and the nanorods were redispersed in a selected wash solution. Together, this process constitutes a single washing step. Should an insoluble pellet be observed, vortexing of the solution for ~3 s was employed to ensure that all soluble materials were fully dispersed into solution. To determine the effects of material purity, UV−vis spectroscopy of the Au nanorods was employed after each wash, which is presented in Figure 1. This technique is quite sensitive to the shape and aggregation state of the materials on the basis of the position and shifting of the plasmon bands.[9] Figure 1a specifically presents the stability analysis for the Au nanorods using a wash solution composed of deionized water with no CTAB. The crude materials (black spectrum) displayed two plasmon bands at 505 nm for the transverse surface plasmon and 722 nm for the longitudinal surface plasmon in the visible region of the spectrum, which is consistent with previous studies.[11,37] After one wash step, the materials readily redispersed in the water wash solution and displayed an almost identical spectrum (red plot); however, there was a slight red shift and an intensity decrease associated with the longitudinal surface plasmon band. This could be attributed to changes in the solution medium (lower surfactant concentration) as well as material loss during the decanting process. Nevertheless, the materials were stable, as the UV−vis data suggested that negligible changes in the nanorod structure occurred after the initial wash. The materials were washed for a second time (green plot), from which only minor changes in the spectrum were again observed as compared to the one wash sample. The nanorods studied after a third wash displayed significant changes. In this sample, only a fraction of the pellet redispersed, whereas a majority of the materials remained as a dark-black precipitate, which is indicative of bulk aggregate formation. The analysis of the redispersible materials (blue spectrum) demonstrated a substantially broadened and red-shifted longitudinal surface plasmon peak. This broadening and shifting indicates that the materials may have aggregated to form larger structures. Subsequent washing steps on these materials were studied; however, no significant absorption was noted in the UV−vis spectra. This is likely due to bulk

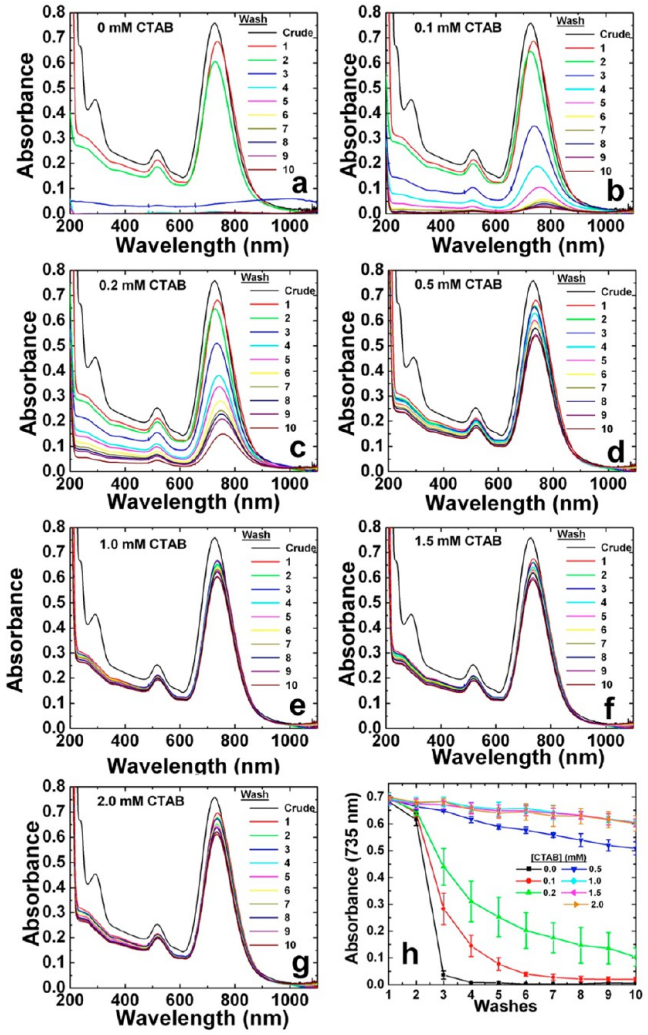

Figure 1. UV−vis analysis of the effect of washing Au nanorods with a CTAB solution of (a) 0, (b) 0.1, (c) 0.2, (d) 0.5, (e) 1.0, (f) 1.5, and (g) 2.0 mM. Panel h presents the decrease in the longitudinal surface plasmon absorbance as a function of the wash number for each CTAB concentration.

aggregation with minimal material dispersion below the UV−vis detection limit, but it is noted that some materials were dispersed, as indicated by DLS analysis (discussed later).

A changing of the wash solution to 0.1 mM CTAB was subsequently used to stabilize the materials for extended washing cycles. As shown in Figure 1b using 0.1 mM CTAB, similar spectra were observed for the materials after two washing steps as compared to the water-based analysis (green spectrum); however, after the third wash (blue spectrum), redispersible materials were achieved in this system. For this, a longitudinal surface plasmon was maintained at 739 nm, which is slightly red-shifted by 14 nm compared to the materials after the second wash. Furthermore, a small insoluble pellet does remain for these materials after three washes; however, it is smaller compared to the water-based system. Subsequent washes demonstrated that a fraction of the materials were redispersible in the 0.1 mM CTAB wash solution, but a continual slight red shift in the longitudinal surface plasmon position was observed after each wash. This shifting and intensity decrease was sustained until only a minor absorbance was noted after five wash steps (pink spectrum). Subsequent

dx.doi.org/10.1021/am401997q | ACS Appl. Mater. Interfaces 2013, 5, 7906−7914

washes using 0.1 mM CTAB displayed only minimal absorbances. Under the same conditions employing a 0.2 mM CTAB wash solution (Figure 1c), similar results to the 0.1 mM CTAB system were noted; however, dispersible materials were observed even after 10 centrifugation cycles with a small insoluble pellet consistently noted after each wash. Although dispersible materials were present, it likely constituted only a fraction of the total sample because of the large decrease in longitudinal surface plasmon absorbance.

When the CTAB concentration in the wash solution was increased to 0.5 mM (Figure 1d), a significant change in the UV−vis profile was observed. In this sample, although a decrease in the absolute intensity of the longitudinal surface plasmon was noted (0.212 absorbance units after 10 washes), minimal to no shifting in the peak position was observed after the washing process began. In addition, the intensity decrease was substantially smaller than those observed with lower CTAB concentrations, and the materials were fully dispersible with no noticeable pellet even after 10 washing cycles. At subsequently higher CTAB concentrations between 1.0 mM and 2.0 mM (Figures 1e−g), a nearly identical UV−vis profile was observed for the Au nanorods after each washing step, with only nominal changes in the spectra after 10 cycles. The minor peak shifts between the crude and washed materials likely arise from changes in the CTAB concentration, altering the dielectric constant of the solution. For these materials, the Au nanorods were fully redispersible in the wash solutions, no significant longitudinal surface plasmon peak shifts were noted, and only minor absorbance decreases were observed, which were likely due to sample loss during supernatant decanting. It is interesting to point out that the critical micelle concentration (CMC) for CTAB is 1 mM,[39] which is the same concentration where enhanced stability is observed after all purification cycles. Figure 1h presents the intensity profile of the longitudinal surface plasmon peak for all seven samples. In this plot, it is evident that major changes were noted for the 0.0, 0.1, and 0.2 mM wash-solution systems, as the decrease in the longitudinal surface plasmon intensity is large. Note that the actual rate of absorbance decrease as a function of the number of washes diminishes with increasing CTAB wash-solution concentrations. At CTAB concentrations ≥0.5 mM, the longitudinal surface plasmon intensity decrease is substantially diminished, suggestive of increased materials stability.

To validate these observations, further analytical characterization methods including TEM, ζ-potential, and DLS analyses were performed. TEM images of the crude sample could not be obtained because of the high CTAB concentration in the reaction. Figure 2 presents the TEM images of the Au nanorods after washes one, three, and six using wash solutions with CTAB concentrations of 0.1, 0.2, 0.5, and 1.0 mM. TEM images of all stable materials after all washes are presented in the Supporting Information, Figures S1−S10. The TEM images of the materials washed with 0.1 mM CTAB are shown in Figure 2a. After one wash, Au nanorods were observed with an aspect ratio of 2.8 ± 0.6, which is consistent with previous results on the basis of the concentration of seeds in the nanorod growth solution.[2,11,37] Interestingly, after additional washes, Au nanorods of similar aspect ratios were observed; after washes three and six, the nanorods possessed aspect ratios of 3.3 ± 1.0 and 3.6 ± 0.8, respectively. This was quite surprising in light of the formation of an insoluble Au precipitate after the second wash. Furthermore, the UV−vis study demonstrated a shifted longitudinal surface plasmon peak

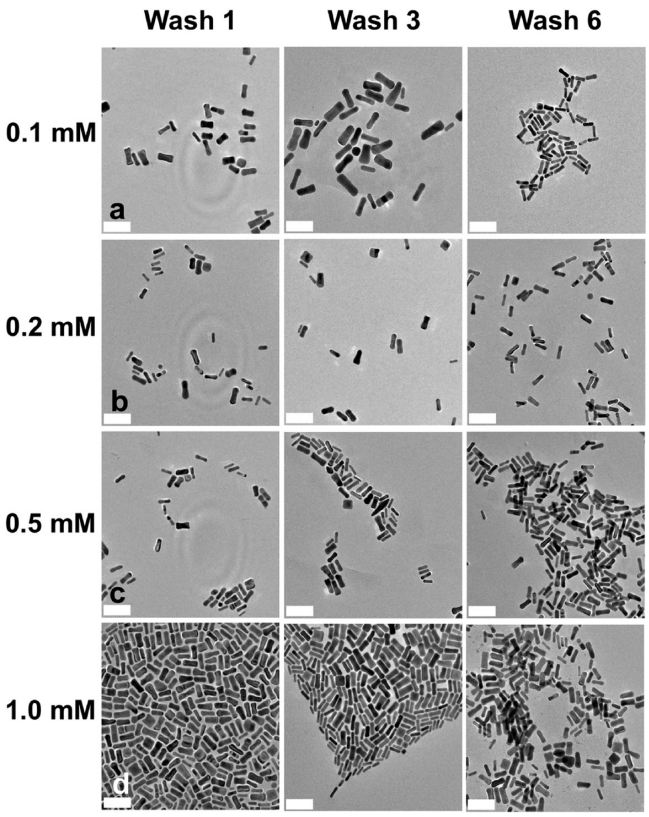

Figure 2. TEM images of the Au nanorods after CTAB washes one, three, and six with a CTAB concentration of (a) 0.1, (b) 0.2, (c) 0.5, and (d) 1.0 mM. The scale bar is 50 nm for all samples.

with significant intensity decreases, all of which are consistent with nanorod aggregation. Similar observations were noted for all of the samples studied by TEM at all CTAB wash-solution concentrations (Figure 2b−d). As is evident from the presented TEM images, Au nanorods were observed in each sample of similar dimensions at the selected CTAB wash concentrations and number of wash cycles completed. Figure 3 displays the

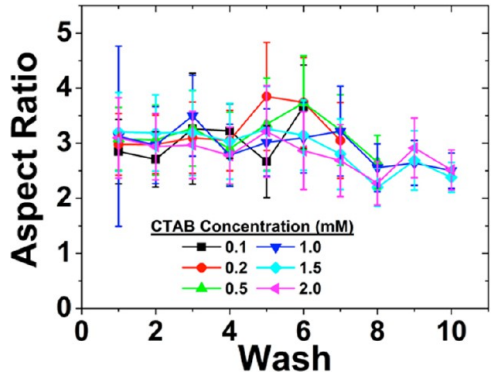

Figure 3. Change in the Au-nanorod aspect ratio as a function of the wash number and CTAB concentration.

aspect ratios for all of the materials studied as a function of the CTAB wash concentration and number of washes. What is evident is that minimal to no substantial changes in the aspect ratio were observed for these samples throughout the washing procedures. Note that aspect ratios could only be achieved for samples in which the Au nanorods were dispersible in solution.

Unfortunately, TEM imaging is unable to study the entire material population for particle size; thus, DLS analysis of each sample after each wash was performed (Figure 4). In general, at

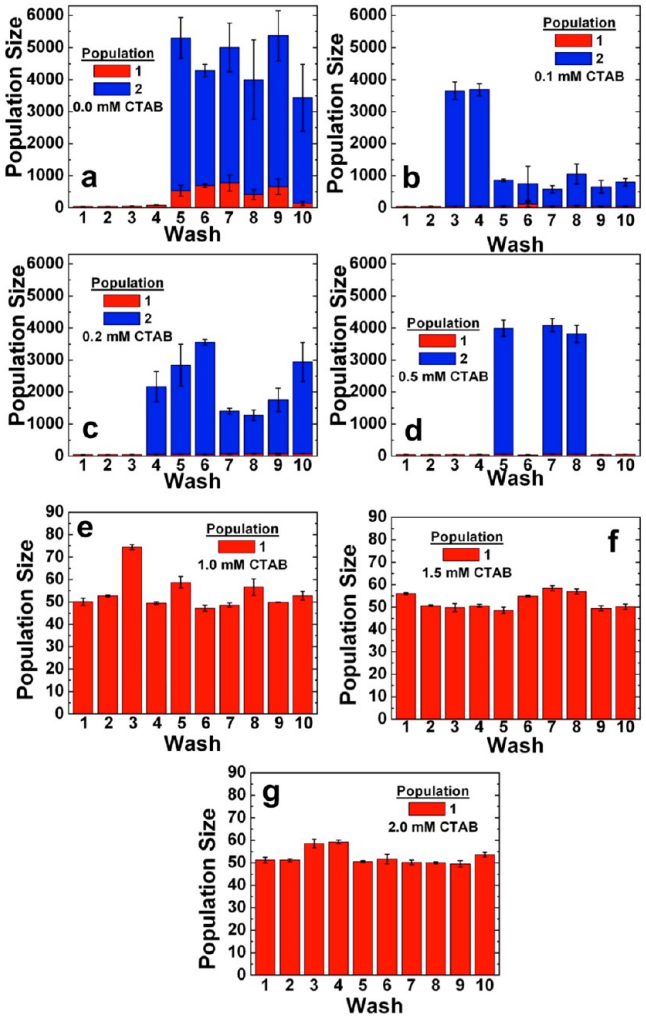

Figure 4. DLS analysis of Au nanorods purified using wash solutions with a CTAB concentration of (a) 0.0, (b) 0.1, (c) 0.2, (d) 0.5, (e) 1.0, (f) 1.5, and (g) 2.0 mM.

the lower CTAB wash concentrations, a bimodal material population was observed; however, at higher CTAB washes, a single-size material was noted after each wash. Figure 4a presents the population analysis for the nanorods washed with 0.0 mM CTAB. In this sample, a single population of 48.9 ± 0.8, 49.8 ± 0.9, 60.9 ± 2.2, and 83.4 ± 5.3 nm was observed after washes one, two, three, and four, respectively, suggestive of minor material aggregation after the second wash. Note that DLS analysis reflects the hydrodynamic radius of the materials in solution and is unable to resolve information concerning particle shape. After wash five, a significant change in particle size was observed wherein two differently sized materials were noted: 533 ± 173 and 4766 ± 638 nm. This trend continued up to the higher washes, which is likely due to bulk aggregation. For the 0.1 mM CTAB wash system (Figure 4b), at lower wash numbers (≤2), particle sizes of 51.3 ± 1.3 and 55.2 ± 0.7 nm were observed. At subsequently higher washes, a bimodal population was again observed. Interestingly, for all of the washes, a particle population size of ∼52 nm was noted, which arises from stable Au nanorods mixed with a second population size of >520 nm. This second population likely corresponds to aggregated materials dispersed in the mixture. Similar observations were noted for the materials washed with 0.2 mM CTAB (Figure 4c) with a bimodal population of materials: one population of a size consistent with the Au nanorods and a second aggregate population.

As the concentration of CTAB increased to 0.5 mM (Figure 4d), an interesting shift the population size of the materials was noted. For instance, at low wash numbers of less than five, only materials with a size expected for the Au nanorods were observed (54.9 ± 0.9, 52.9 ± 0.4, 53.8 ± 1.7, and 55.3 ± 1.4 nm, for washes one−four, respectively). At wash five, a bimodal population was noted with a size of 60.4 ± 4 nm for the stable nanorods and 3936 ± 252 nm for the aggregates. At wash six, a single population with a size of 47.7 ± 1.0 nm was observed; however, after washes seven and eight, a bimodal population of stable Au nanorods and bulk aggregates was again determined. For washes nine and 10, only a single population was observed with a size anticipated for the stable materials. At subsequently higher CTAB wash concentrations (Figure 4e−g), only a single material population is noted, with a size of ∼52 nm. This data suggests that at the higher wash concentrations, Au-nanorod aggregation is inhibited, resulting in stable materials after multiple purification steps. ζ-potential analyses of the different material sets are presented in the Supporting Information, Figure S11. In this study, a general trend of decreasing positive surface charge was noted as a function of the number of washes. Overall, a higher rate of charge decrease was noted for the Au nanorods washed with lower CTAB concentrations, which is consistent with higher degrees of surfactant desorption to reach equilibrium.

Taken together, these results suggest that the Au nanorods are selectively aggregating, which may be based upon the stability of the passivant layer and the number and severity of defects found within the bilayer (Scheme 1). Ligand exchange

Scheme 1. Representative Scheme for the Selective Aggregation of the Au Nanorods on the Basis of the Structure of the CTAB Bilayer

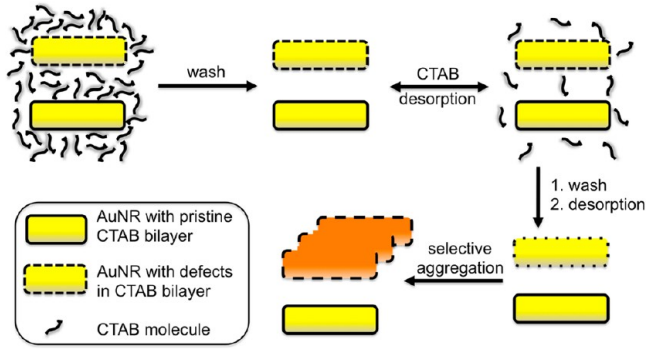

is likely to be enhanced at defect sites because of diminished intermolecular interactions when compared to other sites where the bilayer is intact. When the nanorods are suspended with excess CTAB in the crude reaction solution, defect-based destabilization is minimized because excess surfactant is present that can readily exchange at the site. It may also be possible that the excess surfactant in solution could heal small defects at the Au-nanorod surface, resulting in a pristine bilayer at those locations; however, should sufficiently large bilayer defects be present or if imperfections are located in the Au surface itself,

dx.doi.org/10.1021/am401997q | ACS Appl. Mater. Interfaces 2013, 5, 7906−7914

such a CTAB solution concentration is unanticipated to facilitate reconstruction of the bilayer. Once the materials are washed, the excess CTAB is removed, shifting the equilibrium toward CTAB desorption, increasing the size and number of defects, and diminishing nanorod stability. As the size and numbers of imperfections in the bilayer increase, they expose the Au surface, resulting in material aggregation. Subsequent washes lead to additional CTAB desorption until the nanorods with defective bilayers aggregate and eventually precipitate as bulk material. For those Au nanorods in the same sample mixture with more pristine surfactant bilayers, although CTAB desorption should occur, the rate of desorption is likely to be lower resulting from stronger intermolecular interactions between the bound molecules, increasing the stability of these materials. This suggests that the nanorods selectively aggregate on the basis of the stability of the CTAB bilayer, giving rise to bimodal material populations of different sizes; however, the number of particles in each population is likely to be dramatically different. This is supported by the UV−vis data where slight red shifting of the plasmon band is noted, arising from the aggregated population mixed with the stable Au nanorods. Note that sufficiently aggregated materials are removed from the system in the insoluble pellet; thus, smaller aggregates, likely of low concentration, are dispersed with a higher concentration of Au nanorods in the medium to give rise to the minor peak shifts. DLS data further confirmed the bimodal material population, where the combination of the plasmonic properties of the two materials gives rise to the observed spectra. It is important to point out that DLS is biased toward larger-sized particles;[40] thus, the bimodal population is likely dominated by pristine Au nanorods and a substantially smaller population of aggregates. Interestingly, only non-aggregated Au nanorods were noted in the TEM images. This further supports the DLS data, which indicated that the aggregated structures form only a small fraction of the species in solution. Should the aggregates comprise a greater population size, such materials would have been observed by TEM, larger plasmonic shifts would have been noted in the UV−vis analysis, and the smaller-sized Au nanorods would likely not be observed in the DLS on the basis of their smaller degree of light scattering as compared to the aggregated materials. Note that sizing and spectroscopic analysis of the bulk material pellet was unable to be completed; thus, these studies focused only on those materials that were dispersible after each wash cycle.

From this stability theory, those materials with more defective bilayers would be less stable; however, these imperfections may enhance the ability to chemically modify the Au-nanorod surface. To this end, the defects may facilitate chemical substitution of different ligands (i.e., thiols) to the metallic surface over those nanorods with pristine surfactant bilayers. This could, in turn, lead to a mixture of materials with varying degrees of surface functionalization; however, additional studies at the single-particle level are required to confirm this hypothesis.

Au nanorod Polyelectrolyte-Based Stability Analysis. Although the actual toxicity of the Au nanorods is unclear, it is known that desorbed CTAB molecules are toxic to living cells.[27,41] To overcome this limitation, researchers have coated the nanorod surface using PEs via layer-by-layer (LbL) approaches that have been shown to be nontoxic to living cells.[42,43] To this end, various anionic polymers of different molecular weights have been employed; however, it is likely that on/off equilibria are present for both the polymer and CTAB, leading to PE desorption and disruption of the anticipated material surface structure. To determine how polymer composition affects material stability, Au nanorods coated with two different polymers (PAA and PSS) of different molecular weights were studied.

To probe the PE-stabilizing effects on Au nanorods, the materials were washed with water to remove excess CTAB. In this sense, the materials were centrifuged to form a pellet and then resuspended in an aqueous solution containing the PE and NaCl. The samples were then incubated while shaking on a thermomixer at room temperature for 2.0 h prior to use. The stabilizing effects of the PE coat were determined using UV−vis spectroscopy, where the analysis of the PAA-coated Au nanorods is presented in Figure 5, panels a and b. Figure 5a

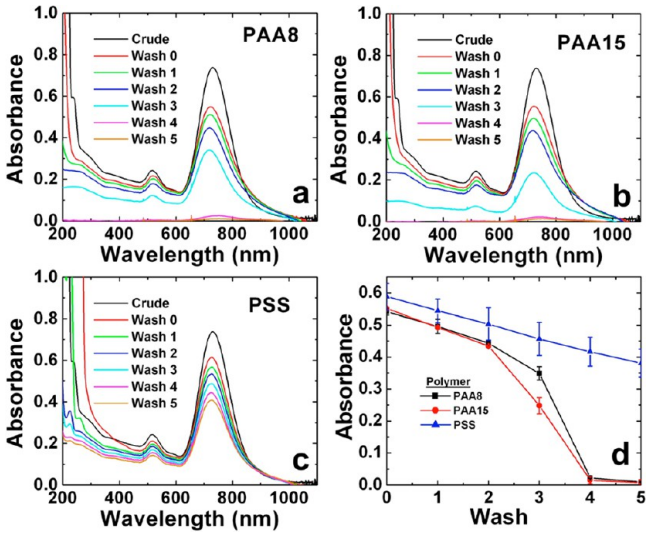

Figure 5. Purification analysis of the Au nanorods coated with (a) PAA8, (b) PAA15, and (c) PSS. Panel d displays the decrease in the longitudinal surface plasmon absorbance of the PE-coated Au nanorods as a function of the wash number.

displays the UV−vis study of the materials coated with PAA8 (MW = 8000 g/mol). After polymer coating (red spectrum), an intensity decrease, a slight blue shift in the longitudinal surface plasmon from 731 nm in the crude sample to 722 nm, and nominal peak broadening were observed after PAA coating. This was likely due to sample loss during nanorod purification and electronic changes at the material surface resulting from the LbL coating, as observed previously;[3,44] however, negligible structural changes may also be possible. Once the PAA-coating process was complete, the materials were washed several times with water, as described earlier. After the first wash, the nanorods remained readily redispersible in water and displayed an almost identical spectrum as compared to the unwashed materials (green spectrum). Further shifting in the longitudinal surface plasmon and a decrease in intensity were observed after a second and third wash (dark- and light-blue spectra, respectively), with the formation of an insoluble black precipitate forming after each wash, indicative of bulk material aggregation. Upon further purification cycles, only a minimal amount of the Au nanorods was redispersible with a minor longitudinal surface plasmon absorbance, whereas a majority of the materials remained as an insoluble dark-black pellet.

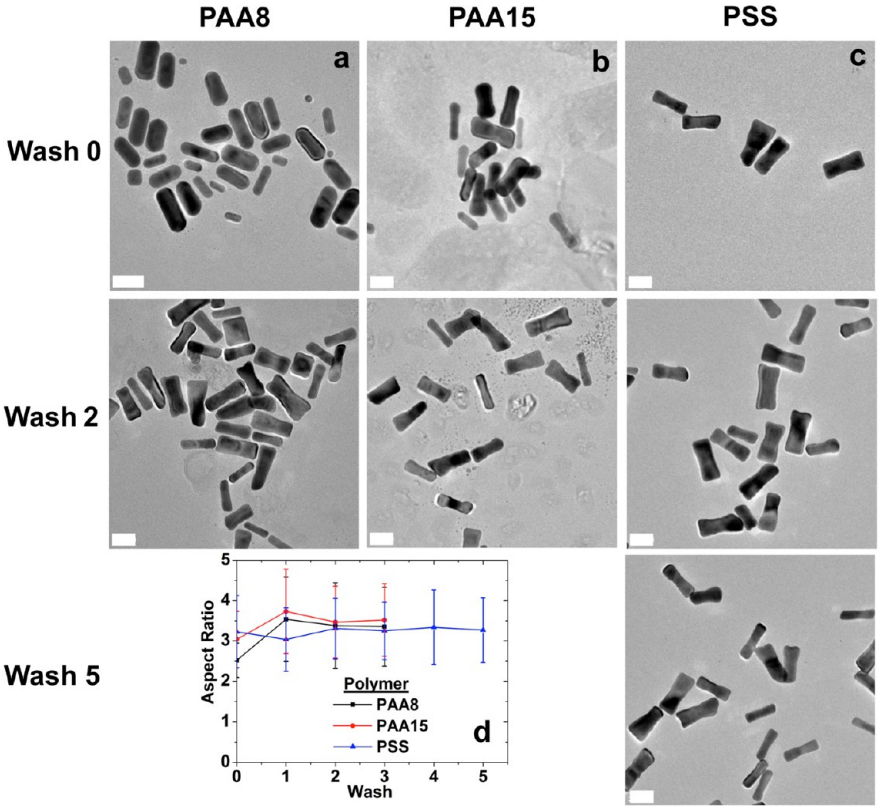

Figure 6. TEM analysis of the PE-coated Au nanorods after washes zero, two, and five. The Au nanorods are coated with (a) PAA8, (b) PAA15, and (c) PSS. Panel d presents the change in the Au-nanorod aspect ratio as a function of the wash number. The scale bar is 40 nm for all samples.

The effects of the PE molecular weight and identity were then studied first by coating the Au nanorods with PAA15 (MW = 15 000 g/mol) (Figure 5b). Similar trends were observed with the PAA15-coated materials as compared to the PAA8 nanorods via UV−vis analysis. To this end, the Au nanorods remained stable and readily redispersible for up to three washes after PE coating with minimal shifting in the longitudinal surface plasmon band. After three wash cycles, the materials were unable to be redispersed, with a nominal longitudinal surface plasmon absorbance. As shown in the Supporting Information, Figure S12, when PAA100 was employed (MW = 100 000 g/mol), although PE-coated Au nanorods were likely produced, the structures were challenging to redisperse after the initial washing procedure. This effect was manifested as a dramatically altered UV−vis spectrum of the materials after washing; thus, no further investigation of their structure was conducted. Interestingly, when the PE structure was changed to PSS (MW = 75 000 g/mol), different degrees of materials stability were noted, as shown in Figure 5c. After polymer functionalization (red spectrum), a small decrease in the longitudinal surface plasmon absorbance was observed with a negligible blue shift of 2 nm, which is consistent with the coating of the materials. After five washes, only a small decrease in the longitudinal surface plasmon absorbance was noted (~0.20 absorbance units), with nominal peak shifting. Furthermore, after each washing cycle, the sample was fully redispersible in water with no formation of an insoluble pellet. Figure 5d presents the longitudinal surface plasmon intensity profile for the materials coated with PAA8, PAA15, and PSS after all five wash cycles. Here, the differences in particle stability were evident with a sharp decrease in the longitudinal surface plasmon intensity of the PAA8- and PAA15-stabilized Au nanorods after the third wash, whereas only a small decrease was noted for the PSS-based materials. This suggests that the PSS polymer system may increase material stability for the PE-coated Au nanorods.

TEM analysis of the PE-coated Au nanorods was also performed to observe any structural changes after each wash cycle. Figure 6 presents images of the materials after zero, two, and five washes, whereas the TEM micrographs for all stable materials can be found in the Supporting Information, Figures S13−S15. Imaging of the PAA8-coated nanorods (Figure 6, panels a and b) indicated that the materials retained their rodlike structure with an aspect ratio of 2.52 ± 0.47, which is consistent with no changes in the morphology after the LbL-coating process. After washes one, two, and three, similar materials with nearly identical aspect ratios of 3.54 ± 1.04, 3.38 ± 1.06, and 3.36 ± 0.98, respectively, were observed. Such a negligible change in nanorod morphology was anticipated on the basis of the minor differences in the longitudinal surface plasmon peak after each wash process. Similar trends were noted for the samples coated with PAA15 and PSS after three washes, as studied by TEM. For the PSS-coated nanorods, however, additional analysis after five washing cycles was possible because of the enhanced stability observed via UV−vis. In this regard, after the fifth wash, Au nanorods with an aspect ratio of 3.27 ± 0.80 were observed. For comparison, Figure 6d illustrates the aspect ratio for each sample on the basis of the PE identity and number of washes. From this analysis, it is evident that no noticeable change to the material aspect ratio was observed as a function of the material purification.

To study further the noted differences between the selected PE-stabilized Au nanorods, DLS and ζ-potential analyses were performed, as presented in Figure 7. Note that when comparing

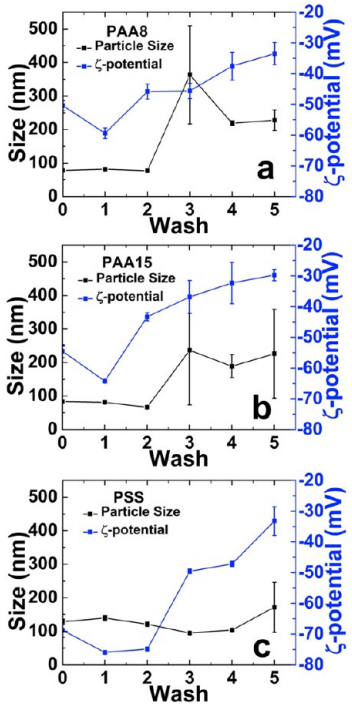

Figure 7. DLS and ζ-potential analysis for the Au nanorods coated with (a) PAA8, (b) PAA15, and (c) PSS.

the size of the PE-coated nanorods to the uncoated materials, a size increase was observed, which is consistent with the changes at the material surface via the LbL coating. Analysis of the PAA8-stabilized materials is specifically presented in Figure 7a. For this sample, the observed hydrodynamic radius of the nanorods immediately after PE coating was 78.2 ± 0.8 nm. After two wash cycles, minimal changes in material size are observed: 81.7 ± 4.9 and 77.4 ± 4.1 nm after washes one and two, respectively. After subsequent wash cycles, larger aggregates were observed, indicating particle instability and aggregation. Similar size-based observations were noted for Au nanorods stabilized with PAA15 (Figure 7b) in which the particle size remained stable after washes zero, one, and two, with material dimensions of 83.4 ± 1.8, 81.1 ± 1.3, and 66.4 ± 1.2 nm, respectively. After wash three, the average hydrodynamic radius increased to 236 ± 163 nm, which continued to increase after subsequent washes. Analysis of the PSS-coated Au nanorods after each wash indicated no significant changes in the particle size for up to five purification cycles (Figure 7c). ζ-potential analysis of each PE-coated Au-nanorod sample is also shown in Figure 7. For each sample, a general trend was observed that demonstrated an increase in surface charge as a function of wash number. Such an effect is likely due to desorption of the negatively charged PE, resulting in exposure of the positive surface charge from the initial CTAB surfactant.

Taken together, the results for the PE-coated materials indicate that the composition of the polymer plays an important role in material stabilization. When looking at materials coated with polymers of identical structure but varying molecular weight (PAA8 and PAA15), minimal differences were noted in the stability. Throughout the first two wash cycles, both systems presented identical UV−vis spectra, indicating similar Au-nanorod structures were present. After the third wash, however, both material systems became unstable, leading to bulk aggregation. In general, lower stability from the PAA materials was evident as compared to the PSS structure. For those Au nanorods coated in PSS, long-term solution stability was evident. For this, no significant change in nanorod dimensions was noted after five purification cycles, as was evident from UV−vis, TEM, and DLS, suggesting enhanced stability. Such effects may arise from the interactions of the sulfonate groups with the CTAB of the cationic Au nanorods, which may be stronger as compared to the PAA materials. Additionally, the larger size of the PSS PE may play a role. Note that PAA100 was studied; however, the formation of redispersible and stable PE-coated Au nanorods could not be achieved using this species. Interestingly, no correlation between the surface charge, as measured by the ζ- potential analysis, and stability was evident. To this end, the PSS materials that were stable possessed a similar surface charge as compared to the PAA-coated Au nanorods that were prone to aggregation. This suggests that differences in the nanorod-surface structure may be present that more evenly distributed the charge along the interface, leading to enhanced stability. Such effects could be important for surface functionalization and are presently under consideration.

SUMMARY AND CONCLUSIONS

These results suggest that the defects present within the CTAB bilayer dictate the solution stability of Au nanorods. To this end, Au nanorods with the most defects aggregate to bulk materials, whereas those with more pristine bilayers remain stable in solution. As a result, a bimodal population of materials is likely present in the sample, giving rise to the differences in stability observed. Increased nanorod stability can be achieved via purification via dilute CTAB solutions (0.5−2.0 mM), which provides sufficient free CTAB to readily exchange with desorbed surfactant at defect sites. This could be used to increase the number of chemical modification steps to allow for further functionalization of the Au-nanorod surface that is important to engender the materials with multiple properties. Note that during this purification process, excess free CTAB is present in solution. Such surfactant species may be undesirable in the final application; however, it could be removed by a final purification step immediately prior to use where the materials could be redispersed in the surfactant-free medium of choice. These stability considerations were expanded to probe the effects of PE-coated Au nanorods, where polymer desorption was observed. Such effects can dramatically change the surface structure and charge of the materials, resulting in nanorod destabilization. Taken together, these results are important in designing synthesis strategies to develop multifunctional materials with plasmonic, biological, and other functionalities.

ASSOCIATED CONTENT

Supporting Information

TEM images from each CTAB wash and concentration, ζ-potential analysis for each CTAB sample, TEM images from each polymer-coated sample, and PAA100 stability analysis. This material is available free of charge via the Internet at http://pubs.acs.org.

AUTHOR INFORMATION

Corresponding Author

*Phone: (305) 284-9351. E-mail: knecht@miami.edu.

Present Address

[§]Department of Radiation Oncology, University of North Carolina−Chapel Hill, 101 Manning Dr., Chapel Hill, North Carolina 27514, United States.

Author Contributions

[∥]These authors contributed equally to this work.

Notes

The authors declare no competing financial interest.

■ ACKNOWLEDGMENTS

This research was supported by funds from the University of Miami and the University of Kentucky. M.S. acknowledges a Presidential Fellowship from the University of Kentucky.

■ REFERENCES

(1) Sun, Z.; Ni, W.; Yang, Z.; Kou, X.; Li, L.; Wang, J. *Small* **2008**, *4*, 1287−1292.
(2) Sethi, M.; Joung, G.; Knecht, M. R. *Langmuir* **2009**, *25*, 1572−1581.
(3) Gole, A.; Murphy, C. J. *Langmuir* **2005**, *21*, 10756−10762.
(4) Tang, L.; Casas, J.; Venkataramasubramani, M. *Anal. Chem.* **2013**, *85*, 1431−1439.
(5) Lin, D.; Wu, J.; Ju, H.; Yan, F. *Biosens. Bioelectron.* **2013**, *45*, 195−200.
(6) Tian, L.; Morrissey, J. J.; Kattumenu, R.; Gandra, N.; Kharasch, E. D.; Singamaneni, S. *Anal. Chem.* **2012**, *84*, 9928−9934.
(7) Xia, Y.; Xiong, Y.; Lim, B.; Skrabalak, S. E. *Angew. Chem., Int. Ed.* **2009**, *48*, 60−103.
(8) Huang, X.; Neretina, S.; El-Sayed, M. A. *Adv. Mater.* **2009**, *21*, 4880−4910.
(9) Jain, P. K.; Eustis, S.; El-Sayed, M. A. *J. Phys. Chem. B* **2006**, *110*, 18243−18253.
(10) Kelly, K. L.; Coronado, E.; Zhao, L. L.; Schatz, G. C. *J. Phys. Chem. B* **2003**, *107*, 668−677.
(11) Murphy, C. J.; Sau, T. K.; Gole, A. M.; Orendorff, C. J.; Gao, J.; Gou, L.; Hunyadi, S. E.; Li, T. *J. Phys. Chem. B* **2005**, *109*, 13857−13870.
(12) Gole, A.; Murphy, C. J. *Chem. Mater.* **2004**, *16*, 3633−3640.
(13) Horiguchi, Y.; Honda, K.; Kato, Y.; Nakashima, N.; Niidome, Y. *Langmuir* **2008**, *24*, 12026−12031.
(14) Berry, V.; Gole, A.; Kundu, S.; Murphy, C. J.; Saraf, R. F. *J. Am. Chem. Soc.* **2005**, *127*, 17600−17601.
(15) Ye, X.; Gao, Y.; Chen, J.; Reifsnyder, D. C.; Zheng, C.; Murray, C. B. *Nano Lett.* **2013**, *13*, 2163−2171.
(16) Vigderman, L.; Zubarev, E. R. *Chem. Mater.* **2013**, *25*, 1450−1457.
(17) Ye, X.; Zheng, C.; Chen, J.; Gao, Y.; Murray, C. B. *Nano Lett.* **2013**, *13*, 765−771.
(18) Sethi, M.; Joung, G.; Knecht, M. R. *Langmuir* **2009**, *25*, 317−325.
(19) Yu, C.; Irudayaraj, J. *Anal. Chem.* **2007**, *79*, 572−579.
(20) McLintock, A.; Hunt, N.; Wark, A. W. *Chem. Commun.* **2011**, *47*, 3757−3759.
(21) Jokerst, J. V.; Cole, A. J.; Van de Sompel, D.; Gambhir, S. S. *ACS Nano* **2012**, *6*, 10366−10377.
(22) Yoshida, A.; Uchida, N.; Kometani, N. *Langmuir* **2009**, *25*, 11802−11807.
(23) Mai, Y.; Xiao, L.; Eisenberg, A. *Macromolecules* **2013**, *46*, 3183−3189.
(24) Alkilany, A. M.; Frey, R. L.; Ferry, J. L.; Murphy, C. J. *Langmuir* **2008**, *24*, 10235−10239.
(25) Alkilany, A. M.; Nagaria, P. K.; Wyatt, M. D.; Murphy, C. J. *Langmuir* **2010**, *26*, 9328−9333.
(26) Alkilany, A.; Murphy, C. *J. Nanopart. Res.* **2010**, *12*, 2313−2333.
(27) Alkilany, A. M.; Nagaria, P. K.; Hexel, C. R.; Shaw, T. J.; Murphy, C. J.; Wyatt, M. D. *Small* **2009**, *5*, 701−708.
(28) Murphy, C. J.; Thompson, L. B.; Alkilany, A. M.; Sisco, P. N.; Boulos, S. P.; Sivapalan, S. T.; Yang, J. A.; Chernak, D. J.; Huang, J. *J. Phys. Chem. Lett.* **2010**, *1*, 2867−2875.
(29) Caswell, K. K.; Wilson, J. N.; Bunz, U. H. F.; Murphy, C. J. *J. Am. Chem. Soc.* **2003**, *125*, 13914−13915.
(30) Cao, J.; Galbraith, E. K.; Sun, T.; Grattan, K. T. V. *Sens. Actuators, B* **2012**, *169*, 360−367.
(31) Hu, J.; Lu, L.; He, W.; Pan, J.; Wang, W.; Xiang, J. *Chem. Phys. Lett.* **2011**, *513*, 241−245.
(32) Nikoobakht, B.; El-Sayed, M. A. *J. Phys. Chem. A* **2003**, *107*, 3372−3378.
(33) Oyelere, A. K.; Chen, P. C.; Huang, X.; El-Sayed, I. H.; El-Sayed, M. A. *Bioconjugate Chem.* **2007**, *18*, 1490−1497.
(34) Kah, J. C. Y.; Chen, J.; Zubieta, A.; Hamad-Schifferli, K. *ACS Nano* **2012**, *6*, 6730−6740.
(35) Baniukevic, J.; Hakki Boyaci, I.; Goktug Bozkurt, A.; Tamer, U.; Ramanavicius, A.; Ramanaviciene, A. *Biosens. Bioelectron.* **2013**, *43*, 281−288.
(36) Chen, C.-C.; Lin, Y.-P.; Wang, C.-W.; Tzeng, H.-C.; Wu, C.-H.; Chen, Y.-C.; Chen, C.-P.; Chen, L.-C.; Wu, Y.-C. *J. Am. Chem. Soc.* **2006**, *128*, 3709−3715.
(37) Sau, T. K.; Murphy, C. J. *Langmuir* **2004**, *20*, 6414−6420.
(38) Alkilany, A. M.; Thompson, L. B.; Murphy, C. J. *ACS Appl. Mater. Interfaces* **2010**, *2*, 3417−3421.
(39) Berr, S. S. *J. Phys. Chem.* **1987**, *91*, 4760−4765.
(40) Filipe, V.; Hawe, A.; Jiskoot, W. *Pharm. Res.* **2010**, *27*, 796−810.
(41) Murphy, C. J.; Gole, A. M.; Stone, J. W.; Sisco, P. N.; Alkilany, A. M.; Goldsmith, E. C.; Baxter, S. C. *Acc. Chem. Res.* **2008**, *41*, 1721−1730.
(42) Hauck, T. S.; Ghazani, A. A.; Chan, W. C. W. *Small* **2008**, *4*, 153−159.
(43) Khlebtsov, N.; Dykman, L. *Chem. Soc. Rev.* **2011**, *40*, 1647−1671.
(44) Gole, A.; Murphy, C. J. *Chem. Mater.* **2005**, *17*, 1325−1330.